1   **Direct evidence of a high-concentration basal layer in a submarine turbidity current**

2   **Zhiwen Wang[1], Jingping Xu[2,3], Peter J. Talling[4], Matthieu J.B. Cartigny[4], Stephen M.**

3   **Simmons[5], Roberto Gwiazda[6], Charles K. Paull[6], Katherine L. Maier[7], Daniel R. Parsons[5],**

4   [1]College of Marine and Geosciences, Ocean University of China, 238 Songling Rd., Qingdao,

5   Shandong, China, 266100

6   [2]Department of Ocean Science and Engineering, Southern University of Science and

7   Technology, 1088 Xueyuan Rd., Shenzhen, Guangdong, China, 518055

8   [3]Laboratory for Marine Geology, Qingdao National Laboratory for Marine Science and

9   Technology, Qingdao, Shandong, China, 266061

10   [4]Department of Earth Sciences and Geography, University of Durham, South Road, Durham

11   DH1 3LE, United Kingdom

12   [5]Energy and Environment Institute, University of Hull, Cottingham Road, Hull HU6 7RX,

13   United Kingdom

14   [6]Monterey Bay Aquarium Research Institute, 7700 Sandholdt Rd., Moss Landing, CA 95039,

15   USA

16   [7]Pacific Coastal and Marine Science Center, U.S. Geological Survey, 2885 Mission St., Santa

17   Cruz, CA 95060, USA

18   Corresponding author: Jingping Xu (xujp@sustech.edu.cn)

Abstract

Submarine turbidity currents are one of the most important sediment transfer processes on earth. Yet the fundamental nature of turbidity currents is still debated; especially whether they are entirely dilute and turbulent, or a thin and dense basal layer drives the flow. This major knowledge gap is mainly due to a near-complete lack of direct measurements of sediment concentration within active submarine flows. Here we present the most detailed near-bed sediment concentrations measurements from a powerful turbidity current in Monterey Canyon, offshore California. We employ a novel approach using correlations between conductivity and sediment concentration, which unlike previous methods can measure very high concentrations and not sensitive to grain size. We find that sediment concentrations close to the canyon floor gradually increased after the arrival of the turbidity current, until reaching a maximum value of 12%, the highest concentration ever inferred from direct measurements in turbidity currents. We also show a two-layer flow head, with a fast (up to 4 m/s), thin and dense basal layer overlain by a thicker (~50 m) dilute flow. At the interface of these two layers, there seems to be a sharp steep concentration gradient. Such quantitative measurements of sediment concentration can produce a key step forward in understanding the basic character and dynamics of these powerful submarine flows.

Keywords: Turbidity currents; Sediment concentration; Seawater conductivity; Monterey canyon

1 Introduction

Whether high sediment concentration layers occur at the base of turbidity currents has long been debated (Kuenen and Migliorini, 1950; Middleton, 1967; Lowe, 1982; Postma et al.,

2

1988; LeClair and Arnott, 2003; Talling et al., 2012). The controversy mainly focuses on whether these submarine flows are entirely dilute (<< 1-2% by volume) and fully turbulent, perhaps with a bedload layer just a few grains thick (as is the case for almost all rivers), or whether a dilute layer overlies a much denser (~10-40%), up to several meters thick basal layer that drives the flow (Kuenen and Migliorini, 1950; Sanders, 1965; Lowe, 1982; Middleton, 1993; Kneller and Branney, 1995; Talling et al., 2012). The fundamental differences between entirely dilute flows and flows with dense basal layers are very important because they control flow speed, runout, impact forces on seabed structures or cables, and how flows deposit sediment. This question is hard to answer using flow deposits or physical and mathematical modelling, as dense or dilute flows can potentially produce similar deposits (Talling et al., 2012), whilst initial flow density is a predefined input condition for modelling. Lack of direct measurements in full-scale submarine flows is one of the root causes of the debate.

More recently, rare field observations have provided limited evidence for the multiple layer structure that has been theoretically or experimentally predicted (Middleton, 1969; Garcia and Parker, 1993; Mulder and Alexander, 2001). Hughes Clarke (2016) used multibeam sonars to show a thin (< 2 m) layer of higher sediment concentration within flows at Squamish Delta in British Columbia, and this dense basal layer caused up-slope migration of bedforms. Based on a multibeam sonar image of a turbidity current from the Scheldt River, Netherlands, Clare et al. (2015) observed a highly reflective basal layer underlying a more dilute layer. However, these field studies were unable to quantify the density of the basal layers due to lack of direct measurements. Quantifying sediment concentration in the field thus remains a key challenge for understanding what turbidity currents are, and how they work (Bornhold et al., 1994; Clare et al., 2015; Talling et al., 2015, Stevenson et al., 2018).

64   This paper presents evidence of a high-concentration basal layer within a submarine

65   turbidity current in Monterey Canyon. Concentrations as high as 12% by volume were

66   determined innovatively by using a conductivity sensor.

67   We first describe a turbidity current that was recorded on 15 January 2016 by an array of

68   seven moorings and one Seafloor Instrument Node (Paull et al., 2018). This array, extending for

69   50 km along the canyon between 300 and 2000 m water depth (Figure 1), recorded the most

70   detailed measurements yet of submarine turbidity currents. We then show experimental

71   calibrations between sediment concentration and conductivity, which allowed us to calculate

72   sediment concentrations in the basal layer recorded by the MS5 mooring at 1450 m water depth.

73   Finally, we interpret the field results, and discuss the wider implications for better understanding

74   turbidity currents.
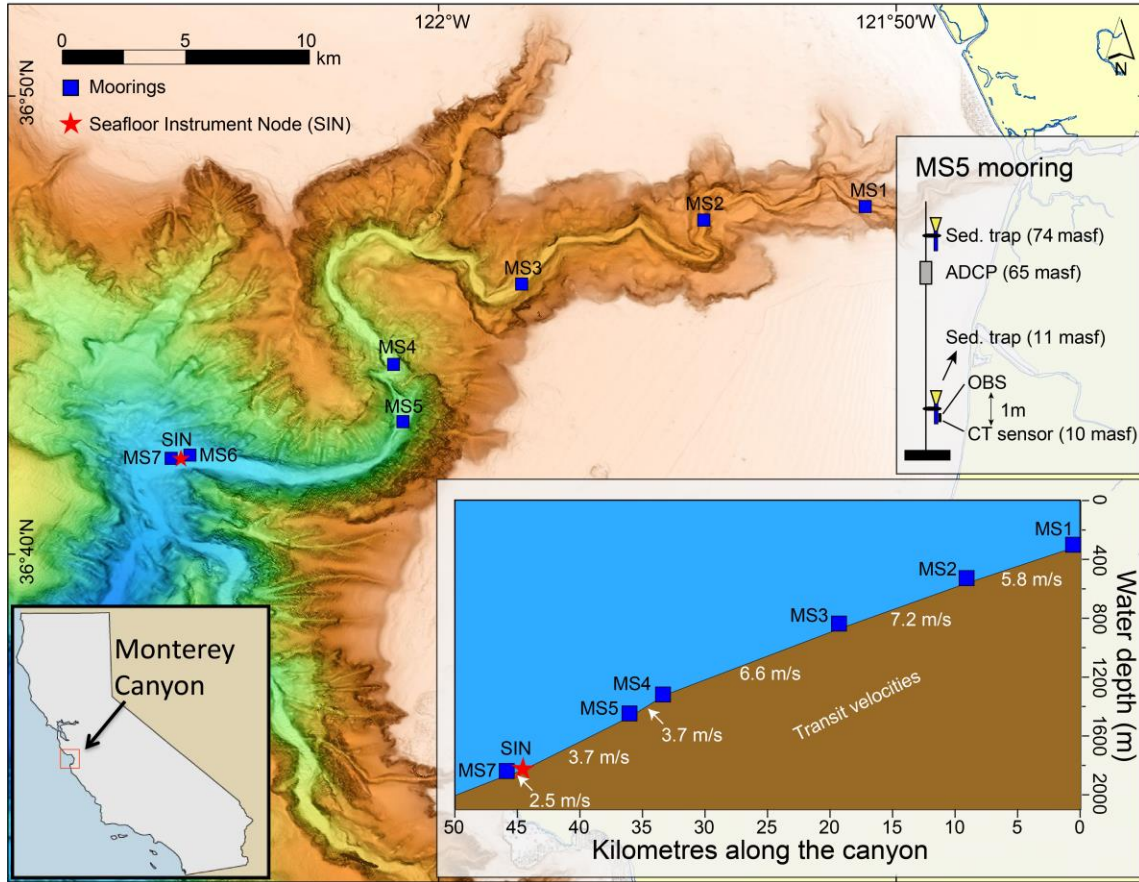
Figure 1. Location map of Monterey Canyon showing the seven moorings, and one seabed frame (SIN), along the submarine canyon. Axial bathymetric profile, with mooring sites, along the canyon are shown in the inset at the lower right. Transit velocities (white numbers) of the 15 January 2016 flow are calculated from distance along the canyon-floor thalweg, and difference in arrival time between moorings. The mooring configuration for MS5 is shown by the mooring conceptual diagram.

2 Turbidity Current Event on 15 January 2016

The turbidity current was recorded by 7 moorings (Figure 1) that were equipped with Acoustic Doppler Current Profiler (ADCP), Conductivity/Temperature (CT) sensors, optical backscatter sensors (OBS), and sediment traps. The general character of the flow was previously

86 reported by Paull et al. (2018). And in this study, we only focus the data of the mooring at 1450

87 m (MS5), the RBR® CT sensor on which recorded a conductivity anomaly during the event that

88 allowed us to apply a novel approach of quantifying the super-high sediment concentration. The

89 initial thickness of the flow estimated by the ADCP was about 20 m (Figure 2A). Thus, CT

90 sensor mounted 10 meters above sea floor (masf) and OBS mounted 11 masf were well inside

91 the body of the flow (Figure 1). At the arrival of the flow, the measured turbidity increased very

92 quickly to reach a peak value of over 800 NTU (nephelometric turbidity units) before gradually

93 returning to pre-event level (Figure 2C). At the same time, the measured conductivity of turbidity

94 current rapidly decreased, by as much as 30%, before it gradually returned to pre-event values

95 over the next three and a half hours (Figure 2D). Temperature increased by as much as 1℃

96 during the same period. The transit velocities of the flow ranged between 2.5 and 7.2 m/s, and

97 averaged 5.4 m/s for the stretch of the canyon occupied by the mooring array (Paull et al., 2018;

98 Figure 1). The maximum instantaneous velocity measured by the MS5 ADCP was 4.1 m/s (Paull

99 et al., 2018), and the transit speed here is 3.7 m/s (Figure 1). They are by far the fastest velocities

100 directly measured by moored sensors in submarine flows (Xu et al., 2004, 2014). The entire

101 turbidity current lasted about 6 hours (Figures 2A and 2B).

102   Two sediment traps on MS5, at 11 and 74 masf, collected sediment in the flow (Figure

103 1). The lower trap contains coarser sand than the upper sediment trap (Maier et al., 2019).

104 Because the thickness of the flow is much less than 70 m, judging from the ADCP measured

105 flow structure, sand in the upper trap either came from the billows in the flow or clouds that

106 arrived after the main body of the flow, or the trap was pulled closer to the sea bed (Paull et al.,

107 2018).

108
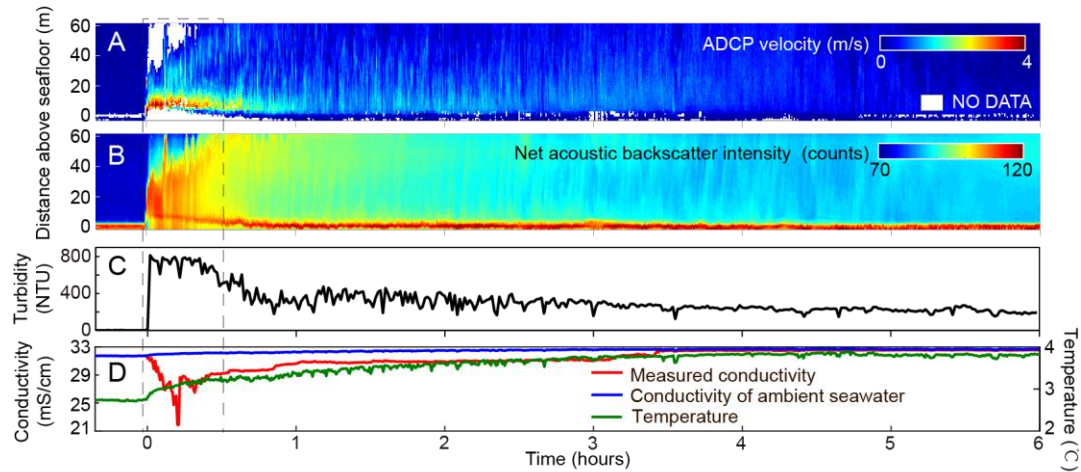
Figure 2. Velocity and echo intensity during 15 January 2016 flow event. A: Time series of flow

speed measured by a downward-looking ADCP initially mounted 65 meters above sea floor

(masf). B: Time series of net acoustic backscatter intensity (averaged over four beams) measured

by the ADCP; the influence of water attenuation and spherical spreading have been corrected. C:

Time-series of water turbidity measured by OBS initially mounted at 11 masf. D: Time series of

temperature (green) and conductivity (red) measured by CT sensor initially mounted at 10 masf.

Conductivity of ambient seawater (blue) was calculated using a standard formula (Poisson, 1980)

by assuming a constant salinity.

3 Conductivity Anomaly and Sediment Concentration Calculations

3.1 Cause of the conductivity anomaly

The most common and direct cause of conductivity decrease is addition of freshwater.

Assuming this is the case for the conductivity anomaly shown in Figure 2D, the volume of the

added freshwater ($V_{freshwater}$) can be estimated by the salinity difference between the ambient

seawater ($S_{seawater}$) and the water mass inside the turbidity current ($S_{turbidity}$):

$$V_{freshwater} = V(S_{seawater} - S_{turbidity})/S_{seawater}, \qquad (1)$$

7

124   where V is the volume of the turbid water mass that can be grossly estimated by simplifying the

125   flow to a cuboid of 50 m (flow depth) × 50 m (canyon width at the MS5 mooring site) × flow

126   length. The flow length can be obtained by multiplying the average flow speed and the duration

127   of the peak flow. Such calculations show that it would require 4.6×10^6 m^3 of freshwater in

128   order to produce the observed conductivity anomaly at MS5. It is almost certain that influx of

129   this much freshwater into the canyon was impossible because: 1) there was hardly any rainfall in

130   the Monterey area during the week before the event; and 2) a sudden release of several millions

131   of cubic meters of fresh groundwater is very unlikely. Thus, the freshwater cause of the

132   conductivity anomaly can be ruled out, and the increase of the temperature (Figure 2D) during

133   the flow was induced by the warmer seawater input from the upstream canyon.

134   Very high sediment content can also cause conductivity decrease because the

135   conductivity of sediment grains is several orders of magnitude smaller than the conductivity of

136   seawater (Traykovski et al., 2000). Applying Archie's law (Archie, 1942) that relates

137   conductivity and volume sediment concentration, we obtain:

138        $$\frac{\gamma_{mixture}}{\gamma_{seawater}} = (1 - C_{sediment})^m, \qquad (2)$$

139   where γ is the conductivity that can be measured by CT sensor, C is the volume concentration,

140   and m is an empirical parameter that ranges from 1.2 to 3.0 (Jackson et al., 1978). Equation (2)

141   would allow us to estimate the sediment concentration C if the constant m becomes known.

142   3.2 Laboratory experiments of estimating m

143   To quantify the relationship between conductivity and sediment concentration (Equation

144   2), a series of laboratory experiments were conducted to measure the variations of conductivity

145   of sea-water and sediment mixtures under different combinations of sediment concentration and

146 temperature conditions. The experiment started with making a saline solution of 34-35‰ by

147 dissolving table salt in a container (bucket#1) with 25 liters of tap water. Roughly 2 kg (dry

148 weight) of sediment was poured into the saline solution while stirring vigorously to make a well-

149 mixed slurry (Figure 3). An incremental scheme of measuring the conductivity of the sediment-

150 water mixture was carried out as follows:
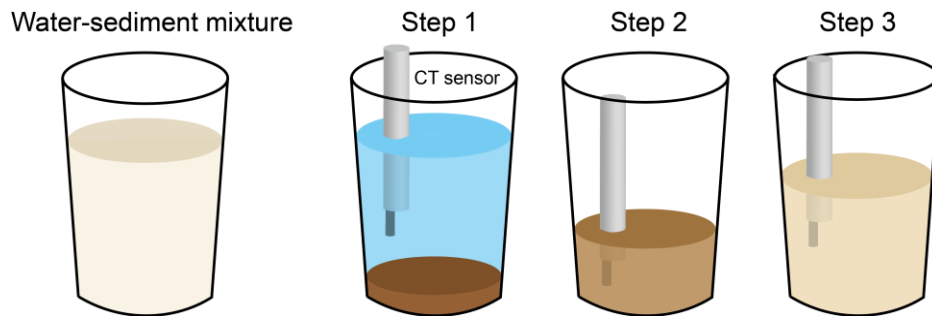
152 **Figure 3.** Interpretive diagram showing the experiment process.

153   1) After all sediment particles had completely settled on the bottom of bucket #1, the

154 salinity, conductivity and temperature of the clear solution in the upper part of the bucket was

155 measured with a RBR® CT sensor (the same type of instrument as used on the mooring during

156 the January 15th flow).

157   2) About 80% of the clear water was removed from bucket#1 to another empty bucket

158 (bucket#2). The remaining mixture of water and sediment in bucket#1 was vigorously stirred to a

159 well-mixed state while continuously measuring the conductivity and temperature of the mixture

160 with the same RBR® CT sensor. A sample of the sediment-water mixture was collected into a

161 small jar for sediment concentration calculation using a drying and weighing method. This first

162 sample had the highest concentration and the lowest conductivity value.

163   3) A small amount of the clear saline water from bucket#2 was added back to bucket#1,

164   vigorously stirred to a well-mixed suspension while continuously measuring the conductivity and

165   temperature. A sample was taken for sediment concentration determination.

166   4) Step 3 was repeated until all the clear saline water in bucket#2 was added back to the

167   mixture in bucket#1. This incremental dilution made the last sample the lowest sediment

168   concentration but the highest conductivity value.

169   Two types of sediment were used in the experiments: finer material (clay) with median

170   diameter of 0.03 mm collected from a mud flat, and coarser sediment (quartz sand) with median

171   diameter of 0.29 mm. Considering that the influence of the sediment content in the seawater to

172   the mixture's conductivity, depend on the ratio of sediment particles' conductivity to the

173   seawater conductivity. And the conductivity of sediment grains is always several orders of

174   magnitude smaller than the conductivity of seawater. Hence, the impacts of the mineralogy of the

175   sediment, which can only influence the absolute conductivity of the sediment grains, are rather

176   limited to the mixture's conductivity changes.

177   The experiments were conducted at room temperature (20-24℃) and in a refrigerated

178   environment (1-4℃). The same procedure (steps 1-4) was repeated for a total of 4 times: 2 grain

179   sizes (fine and coarse) and 2 temperatures (room temperature and refrigerated). The results of

180   these four experiments are listed in Table S1. As shown in Figure 4, the correlation coefficient is

181   0.94 when the empirical exponent m is 2. This suggests that Equation (2) can be used to calculate

182   the sediment concentration from measured conductivity, at least for the range of grain-sizes and

183   temperatures used in these calibration experiments.

184
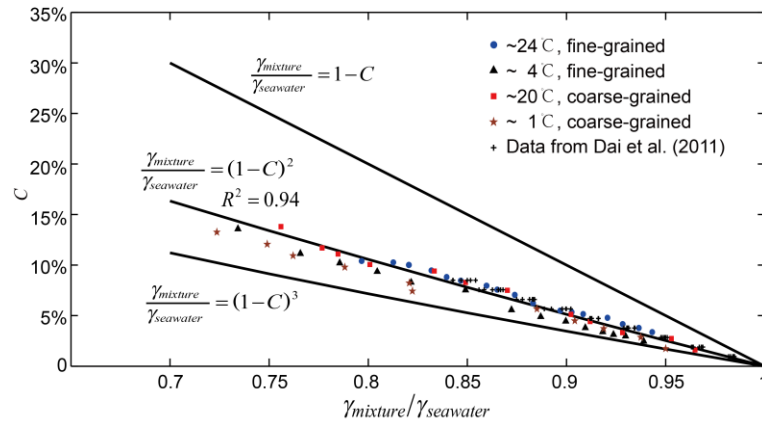
Figure 4. Plot of sediment volume concentration (C) against the conductivity ratio between the sediment-water mixture ($\gamma_{mixture}$) and seawater ($\gamma_{seawater}$). Symbols denote measurements from the four laboratory experiments and a previous calibration dataset from Dai et al. (2011). $\gamma_{mixture}$ was measured with 30 different combinations of environmental factors in Dai's experiment: 2 grain sizes (27 and 52 microns, median diameter), 3 salinities (22‰, 27‰, 32‰), and 5 temperatures (9.2℃, 10.2℃, 15.2℃, 19.2℃, 34.2℃). Solid lines are volume sediment concentrations derived using Equation (2), with $m = 1$, 2, and 3 respectively. $m = 2$ gives the best fit to experimental data.

3.3 Sediment concentration calculations

Assuming seawater salinity throughout the event was constant at the pre-event value (35.4‰), the conductivity of the ambient seawater in the turbidity current (Figure 2D) can be calculated using a standard formula (Poisson, 1980). The ratio between measured and ambient conductivities (Figure 2D) is then used to estimate sediment concentration of the first 30 minutes of the 15 January 2016 flow event (Figure 5A) by Equation (2), with $m = 2$. The rapid decrease of conductivity (i.e. increase of concentration) around minute 12 is believed to result from sensor

200   failure (clogged or partially clogged, see the discussion below for details), therefore the

201   maximum valid concentration is 12% that was recorded at minute 11 (Figure 5A).

202   For comparison, ADCP acoustic backscatter and OBS outputs, both proxies for sediment

203   concentration (Gartner, 2004; Ha et al., 2011), are plotted for the same 30 minutes time window

204   after the arrival of the turbidity current (Figure 5B). It clearly shows that the 26 mS/cm

205   conductivity (maximum sediment concentration) took place about 11 minutes after the arrival of

206   the turbidity current that was marked by the rapid increase of both the ADCP backscatter and the

207   OBS measurements (Figure 5). The measurements of OBS (located 1 m above the CT sensor),

208   which are normally used in dilute flows for estimating sediment concentrations, shows the same

209   pattern as vertically averaged ADCP backscatter (Figure 5B).
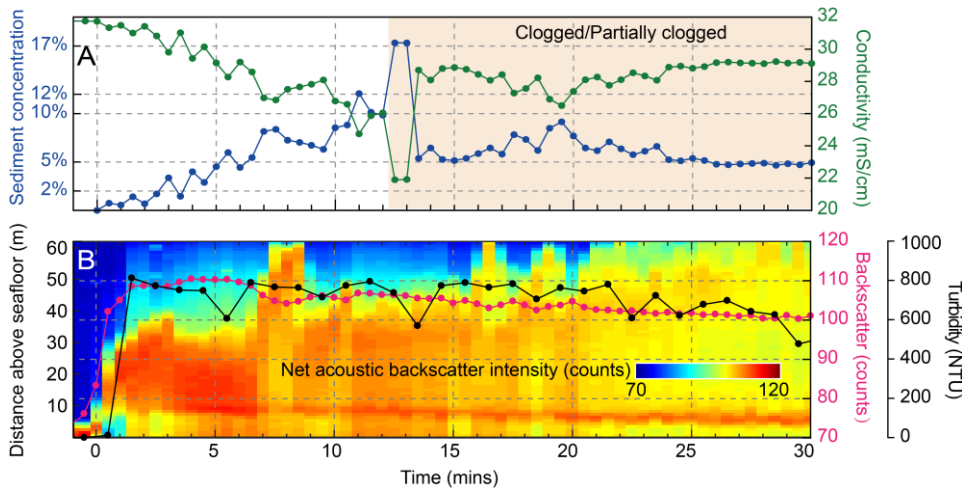
210

211   **Figure 5.** A: Sediment concentration (blue line) converted from the measured conductivity

212   (green line) reduction for the first 30 minutes of 15 January 2016 flow event, using Equation (2),

213   with $m = 2$. The shaded section after minute 12 indicates a clogged or partially clogged sensor.

214   B: Close-up view of the net acoustic backscatter intensity (Figure 2B) for the first 30 minutes of

215   the flow. Overlaid are the vertically averaged acoustic backscatter shown in the red line and the

216 OBS measurements in black. The flow thickness, necessary for the vertical averaging, is defined

217 as: $h = (\int_0^z u dz)^2 / \int_0^z u^2 \, dz$, where z is the height above the bed, u is the flow speed.

4 Discussion

219   This paper describes a new and robust way of measuring high sediment concentrations,

220 however, when used in turbidity currents, its limitation needs to be aware of. This method will

221 not work in environments where the salinity changes appreciably, because we cannot distinguish

222 whether the conductivity decrease in a flow is caused by sediment content or salinity variations.

223 Hence, our approach assumes a constant seawater salinity of 35.4‰ throughout the 15 January

224 2016 flow event. If the salinity measured at the shallower mooring MS1 at 300 m water depth

225 (34.1‰) was used instead for the ambient value, sediment concentration would have been

226 overestimated by a maximum of 1.6 % volume. The actual error would be smaller because of

227 entrainment of saltier water and turbulent diffusion of salt (Zhao et al., 2018) in the head of the

228 flow as it travels down canyon.

229   4.1 Was the CT sensor clogged?

230   The inductive conductivity cell of the RBR$^\circledR$ CT sensor is normally used to measure

231 salinity by allowing seawater to flow freely through the 13 mm diameter hole (with a cross-

232 section area of 1.33 cm^2) in the center of the cell. In some extremely high concentration with

233 coarse grains or clasts, such as near the bottom of turbidity currents, the hole could be clogged or

234 partially clogged by gravel(s) or mud clast(s). Any clogging will reduce the effective cross-

235 section area that will lead to a decrease of measured conductivity (Light et al., 1989).

236
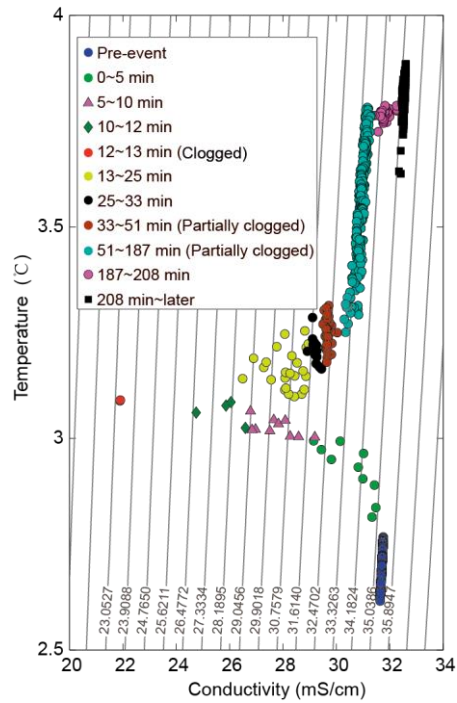
Figure 6. Temperature-conductivity plot of the 15 January 2016 turbidity current (green and red lines in Figure 2D). The measurements were separated into several segments. The thin, parallel lines are isohaline (units: ‰) computed using the formula in Poisson (1980).

The seawater temperature and conductivity at MS5 prior to the arrival of the turbidity current co-vary on a T-C plot along an isohaline corresponding to the ambient salinity of 35.4‰ (Figure 6). After the flow arrived (minute 0-12), the measured conductivity, now affected by the high sediment concentration in the flow, varies independently of measured temperature. Rapid decrease of conductivity between minutes 12 and 13 (Figure 5A) is almost identical to the response of the sensor in laboratory experiment when its cell was blocked by a piece of cardboard (Figure 7), suggesting that the sensor was clogged by coarser sediment or mud clasts. The recovery of the conductivity value from minutes 13 to 24 seems to indicate that the clogging was eased or even completely unclogged. If the latter is the case, it shows that the concentration hovered around 5% for another 11 minutes (Figure 5A). We are not confident about this because

14

250 there is no good explanation why the sensor became unclogged between minutes 13 and 24

251 before it was surely clogged again (see below).

252
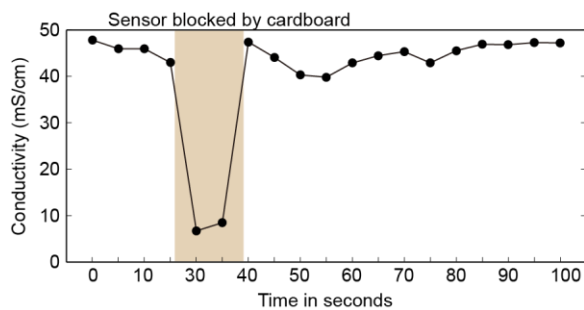
Figure 7. Conductivity readings of the CT sensor in a laboratory experiment with saline water of

254 salinity of 33‰. When the hole of the CT sensor was blocked with a piece of cardboard, the

255 conductivity reading rapidly decreased.

256 From minutes 25 to 33 (Figure 6), however, the measured conductivity and temperature

257 co-varied parallel to an isohaline of much lower salinity (31.8‰). From minutes 33 to 51, the co-

258 variation followed the isohaline of 32.2‰, and from minutes 51 to 187 followed the isohaline of

259 33.3‰. Noticeably both salinities are much lower than the salinity of 34.1‰ measured by a

260 mooring near the head of the canyon. This unusual structure, where the conductivity is off by a

261 fixed amount in each segment, is unlikely due to the high sediment concentration because (1)

262 sediment concentration alone cannot induce the co-variation of conductivity and temperature,

263 and (2) the near bed salinity at the mooring site should be no less than the salinity of the canyon

264 head (34.1‰). Therefore, it is much more likely that the sensor was partially clogged, producing

265 a 'false' signal of low conductivity.

266 All things considered, only the conductivity measurements in the first 12 minutes can be

267 reliably used to estimate sediment concentrations of the turbidity current, which include the

268 maximum concentration that we are confident is valid.

269   4.2 A two-layer system

270   If we apply a Chezy-type model (Bowen et al., 1984), the vertically-averaged

271   concentration inside the flow had to be at least 9% (240 g/l) to maintain the depth-averaged

272   velocity of the turbidity current body measured by the ADCP, assuming no momentum inherited

273   from upslope. Such concentrations would be too high for acoustic penetration by ADCP

274   according to previous studies (Thorne et al., 1993; Shen and Lemmin, 1996), yet the MS5 ADCP

275   recorded valid data throughout the water during the event (Figure 5B). Hence, the high velocity

276   in the flow is more likely due to the presence of a fast-moving, dense, basal-layer that dragged

277   the overlying dilute flow from underneath, which is consistent with the turbidity current

278   travelling model proposed by Paull et al. (2018) and Heerema et al. (2020) based on the

279   movement of very heavy objects and self-acceleration of the flow.

280   To examine the vertical change of sediment concentration, calibrations were applied to

281   convert the recorded OBS values from the engineering units (NTU, Figure 5B) to sediment

282   concentration. For a given concentration, the OBS output was much more sensitive to fine

283   sediments than to their coarse counterpart. For example, it requires a concentration of 2.5% of

284   coarse sediment to produce the same OBS output of 1400 NTU that would only need a mere

285   0.1% concentration for the fine material (Figure 8). Hence, particle size must be determined

286   when the OBS is used as an indirect measure of sediment concentration. According to the

287   sediment collected at 11 masf during the turbidity current, the suspended sediment in the January

288   15 flow contained a wide range of grain sizes (Maier et al., 2019), the 600-800 NTU readings

289   during the first 30 minutes (Figure 5B) could result from a variety of concentrations (Figure 8).

290   However, the 600-800 NTU always represents a dilute flow with the sediment concentration no

more than ~1%, because the grain size of the sediment from the turbidity current (Maier et al.,

2019) was well within the range of calibration experiments.
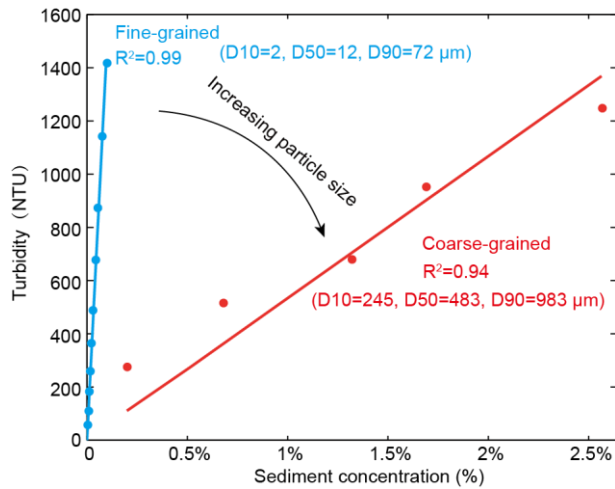
Figure 8. OBS output (NTU) versus sediment concentration from our laboratory experiments

using fine (D50=12 microns) and coarse grained (D50=483 microns) natural sediments. Symbols

denote measurements from the two experiments; solid lines are linear curve fitting.

These observations suggest that the 15 January 2016 turbidity current featured a two-

layer structure, a dense basal layer whose concentration was as 12% or possibly higher, overlain

by a dilute flow with concentration below 1.0%. Moreover, there seems to be a steep

concentration gradient between the basal layer and upper dilute layer because 1) the OBS

recorded a dilute flow during the event, 2) the recovered sediment trap showed no signs of strong

abrasion as might be expected in a dense layer, and 3) parts of the flow imaged by the ADCP

were also dilute ($< 1\%$).

4.3 The 11 minutes delay of the CT measured concentration peak

The discrepancy between the CT-derived sediment concentration (gradual increase until

the sensor was clogged at minute 12) and ADCP backscatter (rapid jump to maximum and then

307   gradually decline) is believed to have resulted from a combined effect of the two-layer structure

308   of the flow, the mooring tilt due to the drag by the very fast flow and the bedform migration (or

309   net deposition).

310   ADCPs measure vertical profiles of the entire water column below. The downward-

311   looking MS5 ADCP recorded the arrival of the flow with a rapid increase of backscatter

312   intensity. In contrast, the CT sensor only records parameters at the height where it is positioned.

313   Moorings of similar design are prone to tilting (Symons et al., 2017), which can move both the

314   ADCP and CT sensor toward the seafloor. We therefore have to determine how far the CT sensor

315   and ADCP were pulled down towards the seabed.
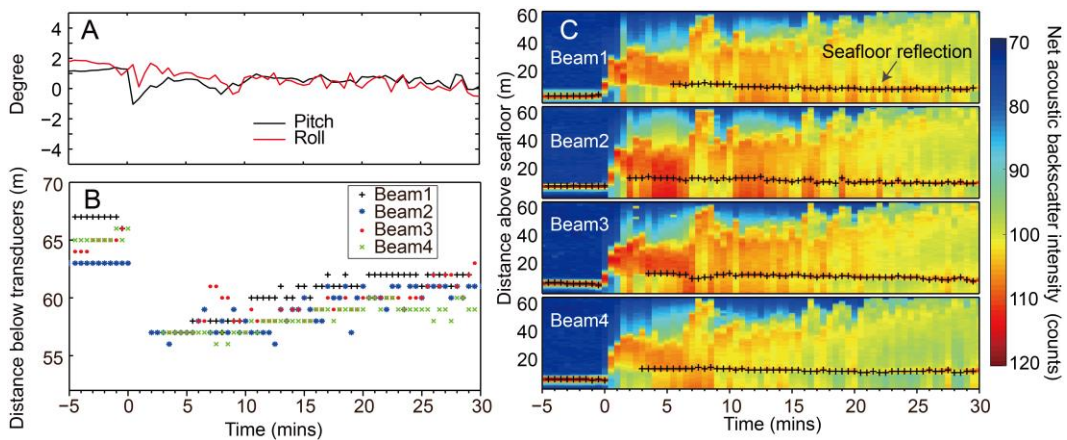
316

317   **Figure 9.** A: ADCP pitch and roll of MS5. B: Location of the highest magnitude acoustic

318   backscatter for all four beams (Beam1~Beam4), which can be used to estimate the position of the

319   seafloor (as shown in C). C: Net acoustic backscatter intensity profiles of individual beams

320   during the first 30 minutes of the flow, the plus signs denote the position of the seafloor echoes

321   Maximum echo intensity of the backscatter signal from the ADCP can be used to

322   estimate the position of the seafloor. The pre-event seabed position was used as the reference for

323   the ADCP profiles. Figure 9C shows the highest magnitude acoustic backscatter for all four

324 beams (Beam1~Beam4). However, during the first 2 minutes of the flow, the ADCP cannot

325 penetrate the high concentrated flow and get clear seafloor echoes, which makes it impossible to

326 estimate the seabed position. But after minute 2, the distance from the ADCP to seafloor was

327 several meters less than its pre-event value (Figure 9B). This could be due to tilting of the

328 mooring by the fast flow, bed aggradation, or both. The pitch and roll (Figure 9A) showed only a

329 very slight wobble when the flow hit the mooring, and the maximum tilt angle of the ADCP was

330 < 2 degrees, which would increase the range to the seafloor by less than ~4 cm. Hence, the

331 ADCP itself is nearly straight when the lower part of the mooring was severely tilted by the flow.

332 The CT sensor was thus estimated to be ~8 m lower than its initial height (10 masf), with an

333 actual height of ~2 masf after the arrival of the flow (minute 2), and gradually rose to ~6 masf at

334 minute 30 (Figure 9B, Figure 10). Because of the assumptions to this approach, these estimated

335 values of sensor's height are not exact, despite the fact that the CT sensor did experience a sharp

336 deepening at the arrival of the flow, before gradually returning to the pre-event position.

337
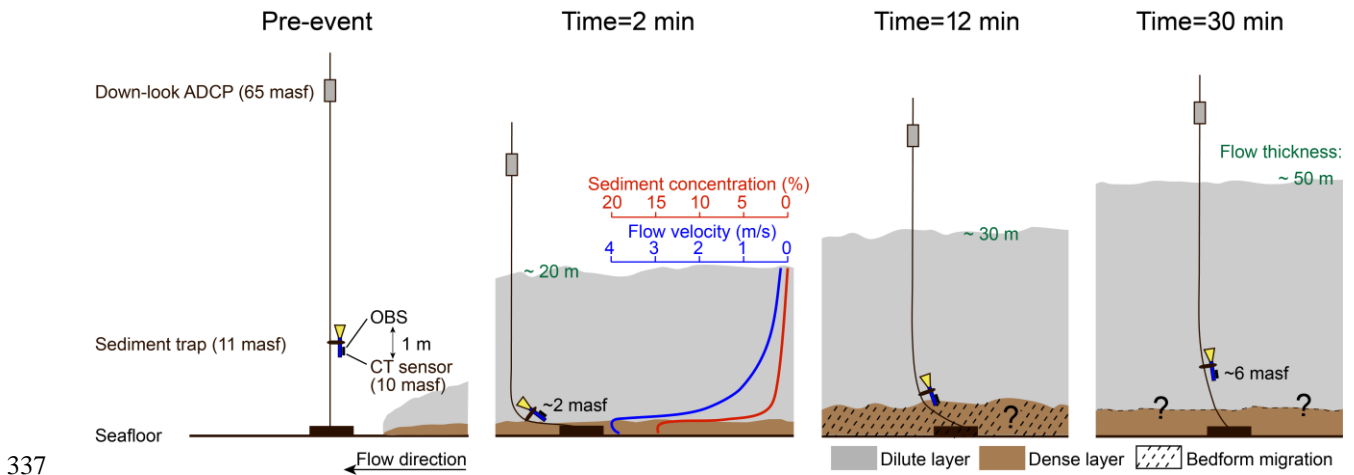
338 **Figure 10.** A conceptual diagram of mooring movement and the two-layer structure of the 15

339 January 2016 turbidity current, inferred from instruments layout on the mooring, ADCP pitch

340   and roll, and the position of the seafloor. The blue and red lines denote the conceptual velocity

341   and concentration profiles within the flow at around 2 minutes after the arrival of the flow.

342   Considering that the mooring didn't moved during the Jan 15 turbidity current because 1)

343   the slight of ADCP sway (pitch and roll) when the flow hits the mooring (Figure 9A), indicating

344   that the mooring didn't experience a hydrodynamic drag on the upper ADCP and floats which

345   would cause the mooring to slant backwards as the anchor moved more rapidly at the base, 2) the

346   ADCP range to seafloor before and after Jan 15 event showed a same bedform (Figure S1). The

347   bathymetric difference of the ADCP beam footprint on seafloor was thus obtained by comparing

348   the distance from the ADCP to seafloor before and after the 15 January 2016 turbidity current

349   (Figure 11), which shows similar magnitudes (±3m) of both erosion and deposition on the circle

350   with ~25 m radius. It seems to show a blue 'trough' (closer to the center) and a red 'crest', both

351   perpendicular to the flow direction, suggesting the presence of a bedform downstream from the

352   mooring, roughly where the sediment trap was pulled down toward the seafloor.

353
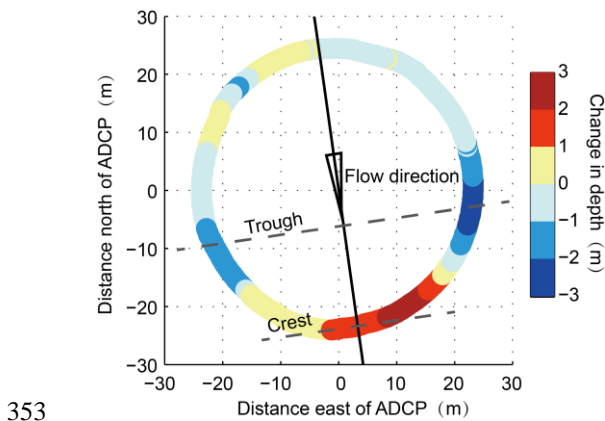
354 **Figure 11**. Bathymetric difference of the ADCP beam footprint on seafloor before and after 15

355 January 2016 turbidity current.

356   Based on the above analyses and the velocity measurements by ADCP, the flow can be

357 inferred to have a two-layer structure with a fast (up to 4 m/s), thin and dense basal layer

358 overlain by a thicker more dilute and slower current. And between the two layers there was a

359 steep concentration gradient (Figure 10). Then the 11 minutes lag between CT-derived maximum

360 concentration and peak ADCP backscatter can be interpreted as follows. About 2 minutes after

361 the arrival of the turbidity current, the thickness of the dilute flow had already reached 20 m.

362 Although the flow was relatively slow at 10 m above the seafloor, the sediment trap package

363 (trap, CT and OBS) was pulled down to the faster flowing layers until the CT sensor at the

364 bottom of the package reached a region just above the dense layer. In this case, the CT sensor

365 recoded the increase in sediment concentration (Figure 5A, Figure 10). Shortly after recording

366 the peak concentration of 12% (minute 11), the CT sensor was clogged at minute 12. It appears

367 that, at this moment, the CT sensor was dipped into the dense layer or even touched the seafloor

368 because of the bedform migration. The CT sensor probably stayed clogged even after rising

369 above the dense layer when the flow began to slow down and the mooring returned upright

370 (Figure 10).

371   The dense near bed layer of the January 15 flow can thus be several meters thick (Figure

372 10), which is consistent with the conceptual model proposed by Paul et al. (2018) and Heerema

373 et al. (2020) that a fast and dense basal layer exists at the flow front, which drives the diluted

374 flow above it. Future work is now needed, but also a challenge, to figure out the actual type of

375 the basal layer, be it a high-density turbidity current (Talling et al., 2012) or special thick

376 bedload layer which is only a few grains thick in rivers (van Rijn, 1984), such as by identifying

377 the deposits form the turbidity current, or via detailed measurements of sediment concentration

378 by ADCP.

379 **5 Conclusions**

380 The 15 January 2016 turbidity current in Monterey Canyon possessed a dense basal layer

381 overlain by a thicker (~50 m) dilute flow. At the interface of these two layers, there seems to be a

382 sharp steep concentration gradient. The maximum sediment concentration in the dense basal

383 layer, measured by a novel conductivity method, was 12%. Concentrations deeper into this layer

384 could have been even higher. The temporal duration and longitudinal length of this dense basal

385 layer remains unknown.

386 The basal layer's presence is consistent with reports of movement of heavy objects at

387 high speeds (Paull et al., 2018), but concentration as high as 12% is the first ever measurement

388 inside the basal layer of field-scale turbidity currents. Understanding whether turbidity currents

389 are entirely dilute and fully turbulent or contain a dilute cloud overlying a thin dense basal layer

390 is critically important because the two types of flows behave in fundamentally different ways,

391 and present very different hazards to seabed structures. Our study also shows how super-high

392 concentrations in basal layer can be successfully measured, thereby provides the necessary

393 means to test turbidity currents models.

References

405 Archie, G.E. (1942), The electrical resistivity log as an aid in determining some reservoir

406   characteristics, Transactions of the American Institute of Mining and Metallurgical

407   Engineers, v. 146, p. 54-62, doi:10.2118/942054-G.

408 Bornhold, B.D., Ren, P., and Prior, D.B. (1994), High-frequency turbidity currents in British

409   Columbia fjords, Geo-Marine Letters, v. 14, no. 4, p. 238–243, doi:

410   10.1007/BF01274059.

411 Bowen, A. J., Normark, W. R., and Piper, D. J. W. (1984), Modelling of turbidity currents on

412   Navy Submarine Fan, California Continental Borderland: Sedimentology, v. 31, no. 2, p.

413   169-185, doi: 10.1111/j.1365-3091.1984.tb01957.x.

414 Catharina J. Heerema, Peter J. Talling, Matthieu J. Cartigny, Charles K. Paull, Lewis Bailey,

415   Stephen M. Simmons, Daniel R. Parsons, Michael A. Clare, Roberto Gwiazda, Eve

416   Lundsten, Krystle Anderson, Katherine L. Maier, Jingping P. Xu, Esther J. Sumner, Kurt

417   Rosenberger, Jenny Gales, Mary McGann, Lionel Carter, Edward Pope (2020), What

418   determines the downstream evolution of turbidity currents?, Earth and Planetary Science

419   Letters, Volume 532, doi: 10.1016/j.epsl.2019.116023.

420   Clare, M.A., Cartigny, M.J.B., North, L.J., Talling, P.J., Vardy, M.E., Hizzett, J.L., Sumner, E.J.,

421   Hughes Clarke, J.E., Fugro, B., and Cooper, C.C. (2015), Quantification of near-bed

422   dense layers and implications for seafloor structures: New insights into the most

423   hazardous aspects of turbidity currents, in Proceedings Offshore Technology Conference

424   2015, p. 4-7, doi:10.4043/25705-MS.

425   Dai, Q., Shan, H. X., Cui, W. L., and Jia, Y. G. (2011), A laboratory study on the relationships

426   between suspended sediment content and the conductivity and their influencing factors

427   [in Chinese with English abstract], Acta Oceanologica Sinica, v. 33, no. 4, p. 88-94.

428   Garcia, M., and Parker, G. (1993), Experiments on the entrainment of sediment into suspension

429   by a dense bottom current, Journal of Geophysical Research Oceans, v. 98, no. C3, p.

430   4793-4807, doi:10.1029/92JC02404.

431   Gartner, J.W. (2004), Estimating suspended solids concentrations from backscatter intensity

432   measured by acoustic Doppler current profiler in San Francisco Bay, California, Marine

433   Geology, v. 211, no. 3, p. 169-187, doi:10.1016/j.margeo.2004.07.001.

434   Ha, H.K., Maa, J.P.Y., Park, K., and Kim, Y.H. (2011), Estimation of high-resolution sediment

435   concentration profiles in bottom boundary layer using pulse-coherent acoustic Doppler

436   current profilers, Marine Geology, v. 279, no. 1, p. 199-209, doi:

437   10.1016/j.margeo.2010.11.002.

438   Hughes Clarke, J. E. (2016), First wide-angle view of channelized turbidity currents links

439   migrating cyclic steps to flow characteristics, Nature Communications, v. 7, p. 11896,

440   doi:10.1038/ncomms11896 (2016).

441 Jackson, P. D., Smith, D. T., and Stanford, P. N. (1978), Resistivity-porosity-particle shape

442   relationships for marine sands, Geophysics, v. 43, no. 6, p. 1250-1268, doi:

443   10.1190/1.1440891.

444 Kneller, B.C., and Branney, M.J. (1995), Sustained high-density turbidity currents and the

445   deposition of thick massive sands, Sedimentology, v. 42, no. 4, p. 607-616, doi:

446   10.1111/j.1365-3091.1995.tb00395.x.

447 Kuenen, P.H., and Migliorini, C.I. (1950), Turbidity currents as a cause of graded bedding,

448   Journal of Geology, v. 58, no. 2, p. 91-127, doi:10.1086/625710.

449 Leclair, S.F. and Arnott, R.W.C. (2003), Coarse-tail graded, structureless strata: indicators of an

450   internal hydraulic jump. In: Shelf Margin Deltas and Linked Down Slope Petroleum

451   Systems: Global Significance and Future Exploration Potential (Eds H.H. Roberts, N.C.

452   Rosen, R.H. Filion, and J.B. Anderson), SEPM, Gulf Coast Section, Houston, p. 817–

453   836.

454 Light, T.S., McHale, E. J., and Fletcher, K. S. (1989), Electrodeless conductivity, Talanta, v. 36,

455   no. 1, p. 235-241, doi:10.1016/0039-9140(89)80101-8.

456 Lowe, D.R. (1982), Sediment gravity flows: II. Depositional models with special reference to the

457   deposits of high-density turbidity currents, Journal of Sedimentary Research, v. 52, no. 6,

458   p. 343-361, doi:10.1306/212F7F31-2B24-11D7-8648000102C1865D.

459 Maier, K. L., Gales, J. A., Paull, C. K., Rosenberger, K., Talling, P. J., Simmons, S. M.,

460   Gwiazda, R., McGann, M., Cartigny, M. J. B., Lundsten, E., Anderson, K., Clare, M. A.,

461   Xu, J., Parsons, D., Barry, J. P., Wolfson-Schwehr, M., Nieminski, N. M., and Sumner,

462   E. J. (2019), Linking Direct Measurements of Turbidity Currents to Submarine Canyon-

463   Floor Deposits: Frontiers in Earth Science, v. 7, no. 144.

464   Middleton, G.V. (1967), Experiments on density and turbidity currents: Ⅲ. deposition of

465   sediment, Canadian Journal of Earth Sciences, v. 4, no. 3, p. 475-505, doi:10.1139/e67-

466   025.

467   Middleton, G.V. (1969), Grain flows and other mass movements down slopes, in Stanley, D.J.,

468   ed., The New Concepts of Continental Margin Sedimentation, American Geological

469   Institute, Short Course Lecture Notes, p. 1–14.

470   Middleton, G.V. (1993), Sediment deposition from turbidity currents, Annual Review of Earth &

471   Planetary Sciences, v. 21, no. 1, p. 89-114, doi:10.1146/annurev.ea.21.050193.000513.

472   Mulder, T., and Alexander, J. (2001), Abrupt change in slope causes variation in the deposit

473   thickness of concentrated particle-driven density currents, Marine Geology, v. 175, no. 1,

474   p. 221-235, doi:10.1016/S0025-3227(01)00114-1.

475   Paull, C. K., Talling, P. J., Maier, K. L., Parsons, D., Xu, J., Caress, D. W., et al. (2018),

476   Powerful turbidity currents driven by dense basal layers, Nature Communications, v. 9,

477   no. 1, p. 4114, doi:10.1594/IEDA/324529.

478   Poisson, A. (1980), Conductivity/salinity/temperature relationship of diluted and concentrated

479   standard seawater, IEEE Journal of Oceanic Engineering, v. OE-5, no. 1, p. 41-50, doi:

480   10.1109/JOE.1980.1145442.

481   Postma, G., Nemec, W., and Kleinspehn, K.L. (1988), Large floating clasts in turbidites: a

482   mechanism for their emplacement, Sedimentary Geology, v. 58, no. 1, p. 47-61, doi:

483   10.1016/0037-0738(88)90005-X.

484 Sanders, J.E. (1965), Primary sedimentary structures formed by turbidity currents and related

485   resedimentation mechanisms, Special Publications, p. 192-219.

486 Shen, C., and Lemmin, U. (1996), Ultrasonic measurements of suspended sediments: a

487   concentration profiling system with attenuation compensation, Measurement Science &

488   Technology, v. 7, no. 9, p. 1191, doi:10.1088/0957-0233/7/9/001.

489 Symons, W.O., Sumner, E.J., Paull, C.K., Cartigny, M.J.B., Xu, J.P., Maier, K.L., Lorenson,

490   T.D., and Talling, P.J. (2017), A new model for turbidity current behavior based on

491   integration of flow monitoring and precision coring in a submarine canyon, Geology,

492   45(4) :367~370, doi:10.1130/G38764.1.

493 Stevenson, C. J., Feldens, P., Georgiopoulou, A., Schönke, M., Krastel, S., Piper, D. J. W.,

494   Lindhorst, K., and Mosher, D. (2018), Reconstructing the sediment concentration of a

495   giant submarine gravity flow: Nature Communications, v. 9, no. 1, p. 2616.

496 Talling, P.J., Masson, D.G., Sumner, E.J., and Malgesini, G. (2012), Subaqueous sediment

497   density flows: Depositional processes and deposit types, Sedimentology, v. 59, no. 7, p.

498   1937–2003, doi:10.1111/j.1365-3091.2012.01353.x.

499 Talling, P.J., et al. (2015), Key future directions for research on turbidity currents and their

500   deposits, Journal of Sedimentary Research, v. 85, no. 2, p. 153-169, doi:

501   10.2110/jsr.2015.03.

502 Thorne, P. D., Hardcastle, P. J., and Soulsby, R. L. (1993), Analysis of Acoustic Measurements

503   of Suspended Sediment, Journal of Geophysical Research C, v. 98, no. C1, p. 899-910,

504   doi:10.1029/92JC01855.

505 Traykovski, P., Geyer, W.R., Irish, J.D., and Lynch, J.F. (2000), The role of wave-induced

506   density-driven fluid mud flows for cross-shelf transport on the Eel River continental

507   shelf, Continental Shelf Research, v. 20, no. 16, p. 2113-2140, doi:10.1016/S0278-

508   4343(00)00071-6.

509 van Rijn, L. C. (1984), Sediment transport, Part I: bed load transport. J. Hydraul. Eng. 110,

510   1431–1456.

511 Xu, J.P., Noble, M.A., and Rosenfeld, L.K. (2004), In-situ measurements of velocity structure

512   within turbidity currents, Geophysical Research Letters, v. 31, no. 9, p. 9311, doi:

513   10.1029/2004GL019718.

514 Xu, J.P., Sequeiros, O.E., and Noble, M.A. (2014), Sediment concentrations, flow conditions,

515   and downstream evolution of two turbidity currents, Monterey Canyon, USA, Deep Sea

516   Research Part I Oceanographic Research Papers, v. 89, no. 3, p. 11-34, doi:

517   10.1016/j.dsr.2014.04.001.

518 Zhao, L., Ouillon, R., Vowinckel, B., Meiburg, E., Kneller, B., and He, Z. (2018), Transition of a

519   hyperpycnal flow into a saline turbidity current due to differential diffusivities,

520   Geophysical Research Letters, v. 45, no. 21, p. 11,875-811,884, doi:

521   10.1029/2018GL080150.